Control of the interparticle spacing in superparamagnetic iron oxide nanoparticle clusters by surface ligand engineering*

Dan Wang(王丹)[1], Bingbing Lin(林兵兵)[1], Taipeng Shen(申太鹏)[1], Jun Wu(吴君)[1], Fuhua Hao(豪富华)[2], Chunchao Xia(夏春潮)[3], Qiyong Gong(龚启勇)[3], Huiru Tang(唐惠儒)[2], Bin Song(宋彬)[3], and Hua Ai(艾华)[1,3,†]

[1] *National Engineering Research Center for Biomaterials, Sichuan University, Chengdu* 610064, *China*
[2] *Wuhan Institute of Physics and Mathematics, Chinese Academy of Sciences, Wuhan* 430071, *China*
[3] *Department of Radiology, West China Hospital, Sichuan University, Chengdu* 610041, *China*

(Received 22 May 2016; published online 1 June 2016)

Polymer-mediated self-assembly of superparamagnetic iron oxide (SPIO) nanoparticles allows modulation of the structure of SPIO nanocrystal cluster and their magnetic properties. In this study, dopamine-functionalized polyesters (DA-polyester) were used to directly control the magnetic nanoparticle spacing and its effect on magnetic resonance relaxation properties of these clusters was investigated. Monodisperse SPIO nanocrystals with different surface coating materials (poly(ε-caprolactone), poly(lactic acid)) of different molecular weights containing dopamine (DA) structure (DA-PCL2k, DA-PCL1k, DA-PLA1k)) were prepared via ligand exchange reaction, and these nanocrystals were encapsulated inside amphiphilic polymer micelles to modulate the SPIO nanocrystal interparticle spacing. Small-angle x-ray scattering (SAXS) was applied to quantify the interparticle spacing of SPIO clusters. The results demonstrated that the tailored magnetic nanoparticle clusters featured controllable interparticle spacing providing directly by the different surface coating of SPIO nanocrystals. Systematic modulation of SPIO nanocrystal interparticle spacing can regulate the saturation magnetization (M_s) and T_2 relaxation of the aggregation, and lead to increased magnetic resonance (MR) relaxation properties with decreased interparticle spacing.

Keywords: nanoparticle clusters, interparticle spacing, ligand exchange, magnetization

PACS: 75.75.–c, 81.16.Dn, 87.61.–c, 87.85.J– **DOI:** 10.1088/1674-1056/25/7/077504

1. Introduction

Magnetic resonance imaging (MRI), one of the commonly used clinical imaging techniques, has been widely applied for assessing a variety of diseases, but it usually requires the assistance of a contrast agent to increase image sensitivity.[1–5] Typically, the contrast agents contain paramagnetic agents and superparamagnetic iron oxide (SPIO) nanoparticles.[6–9] However, paramagnetic gadolinium chelates have low sensitivity and require effective concentration of 10–100 μM for enhanced visualization.[10] SPIO nanoparticles are strong enhancers of proton relaxation with superior MR transverse relaxation (T_2) shortening effects, and can be used at a much lower concentration than paramagnetic agents.[9,11,12] For this reason, considerable interest has been focused on the properties of SPIO nanoparticles including their size, morphology, dopant, coating thickness, and degree of SPIO nanocrystal clustering to obtain high-performance T_2 MRI contrast agents.[13–15]

Control of SPIO nanocrystal aggregation is a well-established method to optimize their T_2 relaxivity. When multiple SPIO nanocrystals are gathered together into clusters, their T_2 relaxivity is greatly improved over single SPIO nanoparticles, leading to a much better signal contrast enhancement.[15,16] Commercial SPIO contrast agents, such as Resovist and Feridex, exhibit enhanced MRI imaging sensitivity and high relaxivities of up to about 150 Fe m·M^{-1}·s^{-1}, due to a high degree of particle aggregation in cell endosomes.[17] Weller suggested that these magnetic clusters are in agreement with the static dephasing regime theory which can result in higher MRI contrast effect.[18] Moreover, T_2 relaxation rate of magnetic clusters depends on the cluster size, and is directly proportional to their size when they are stable colloidal solutions.[19] It is speculated that SPIO nanocrystals' interparticle spacing is a considerable account on influencing the magnetic properties of their nanoclusters, because it plays a significant role in regulating the physical interactions between SPIO nanocrystals and ultimately the magnetization of their aggregation.[20] Understanding of the relationship between SPIO interparticle spacing and relaxivity performance of a collection of SPIO nanocrystals is critical for the design of effective imaging probes and their applications in medical imaging.

Herein, tailored magnetic nanoparticle platform for the controlled assembly of SPIO nanocrytals with different surface coating materials was developed. In order to investigate

*Project supported by the National Key Basic Research Program of China (Grant No. 2013CB933903), the National Key Technology R&D Program of China (Grant No. 2012BAI23B08), and the National Natural Science Foundation of China (Grant Nos. 20974065, 51173117, and 50830107).

†Corresponding author. E-mail: huaai@scu.edu.cn

© 2016 Chinese Physical Society and IOP Publishing Ltd

the magnetic relaxation processes involved in the SPIO interparticle spacing, we modulated nanoparticle interparticle spacing directly by the different surface coating thickness of SPIO nanocrystals. Simultaneously, the coating thickness was varied by changing the length of coating ligands. The tailored nanoparticle formation is illustrated in Fig. 1.

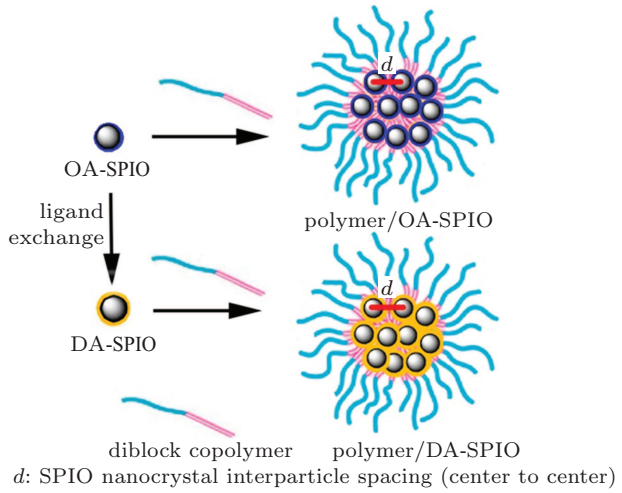


Fig. 1. (color online) Schematic illustration of tailored magnetic nanoparticles formation. The tailored magnetic nanoparticle clusters feature controlled SPIO nanocrystal interparticle spacing of their clusters.

2. Materials and methods

2.1. The synthesis of the versatile anchor and ligand exchange process

The synthesis of the versatile anchor and ligand exchange process are illustrated in Fig. 2. 3, 4-Dibenzyloxyphenethylamine hydrochloride, ε-caprolactone (ε-CL), D, L-lactide, stannous octoate (Sn(Oct)2) were purchased from Aldrich Chemical Co.. 3, 4-Dibenzyloxyphenethylamine hydrochloride (2 g, 5.41 mmol) was dissolved in methylene chloride (DCM, 20 ml) and NaOH aqueous solution (1 M, 5.41 mL, 5.41 mmol) were added. After stirred for 30 min, the organic fractions was sequentially washed by H_2O (3×30 mL), brine (3×30 ml) and dried over anhydrous $MgSO_4$. The resulting products 3, 4-Dibenzyloxyphenethylamine (Bn_2-DA, 1.62 g, 4.87 mmol) was obtained after being filtered and dried.

The ligands were synthesized respectively by ring-opening polymerization of ε-caprolactone (ε-CL) or D, L-lactide using 3, 4-Dibenzyloxyphenethylamine as initiator in anhydrous toluene and stannous octoate ($Sn(Oct)_2$) as a catalyst. A stoichiometric amount of polymeric monomers was added according to the desired molecular weight of exchange ligands. The reaction mixture was stirred at 100 °C for 48 h, and the products were collected by precipitation in

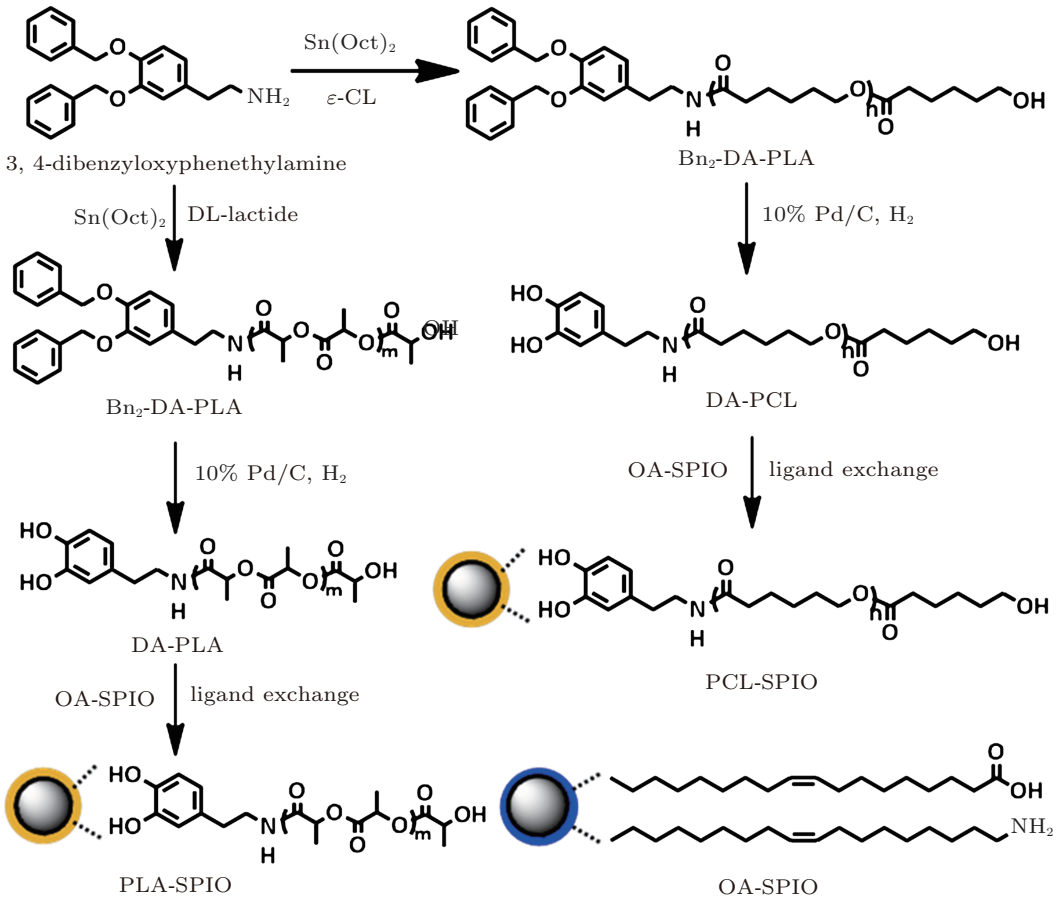


Fig. 2. (color online) The design and synthesis route of the versatile anchor.

diethyl ether under vigorous stirring. In this way, we respectively gained Bn_2-DA-PCL1k, Bn_2-DA-PCL2k, and Bn_2-DA-PLA1k polymers. The removal of benzyl protecting group was carried out in THF/methanol solution with 10% of Pd/C catalyst (0.01 equiv) under 5 atm of hydrogen in an agitated autoclave. After stirred for 72 h at 40 °C, the mixture was filtered, concentrated, dried and obtained DA-capping polymers (DA-PCL1k, DA-PCL2k, and DA-PLA1k). The structure and molecular weight characterization of polymers were confirmed via combined ^{1}H NMR and by gel permeation chromatography (GPC) (HLC-8320GPC, Japan) operating with THF as eluent and calibrated with polystyrene standards.

The monodisperse SPIO nanocrystals (6 nm in diameter) were prepared as described in a previous publication.[21] The ligand exchange of the as-made SPIO nanocrystals with DA-PCL1k, DA-PCL2k, or DA-PLA1k was described as follows. In a 10 mL glass bottle, 10 mg DA-capped polymers was dissolved in 3 mL of dimethyl formamide (DMF), while SPIO nanocrystals ($\sim$ 10 mg) was dispersed in hexane (3 mL). Then the layered solution was placed in an ultrasound bath and sonicated for 30 min. SPIO nanocrystals were then transferred from the upper hexane solution to the lower DMF solution layer. DMF phase was collected and centrifuged at 400000 rpm ($\times$3). The precipitate was redispersed in CH_2Cl_2, and the resulted solution was dialyzed against CH_2Cl_2 to remove residual DMF (MWCO 50 kDa). Finally, these nanoparticles were filtered through 0.22 μm PTFE Acrodisc® syringe filters (PALL Corp.) to remove aggregates.

The size and distribution of SPIO nanocrystals in hexane were evaluated by dynamic light scattering (DLS, Zetasizer Nano ZS, Malvern, U.K.) and transmission electron microscopy (TEM, Tecnai G2 F20 S-TWIN, FEI, US), respectively. Nanoparticle samples for TEM analysis were prepared by drying the dispersion of SPIO nanoparticles on amorphous carbon coated copper grids.

2.2. Self-assembly and characterization of polymer/SPIO nanocomposites

SPIO nanoparticles in hexane were dried under argon flow and redispersed in THF together with polymers. Then, the mixed solution was slowly added into Milli-Q water (produced by Milli-Q Biocel, Milli-pore, USA) with sonication. Using SPIO with different coating layer materials and various copolymers, a series of polymer/SPIO micelles were prepared to regulate the interparticle spacing of SPIO nanoparticles. The mixture was under shaking overnight and THF was removed through rotary evaporation.

Particle size distribution and morphology of micelles were characterized by DLS and TEM (Libra200FE, Carl zeiss, Germany), respectively. Iron concentration from SPIO nanocomposite samples were measured using atomic absorption spectroscopy (AAS, AA800, PerkineElmer, USA) by calculating with a standard curve obtained from iron calibration standard.

2.3. SAXS sample preparation and analysis

SAXS measurements have been used to quantify SPIO nanocrystal interparticle spacing of the nanocomposites using a synchrotron x-ray source, Shanghai Synchrotron Radiation Facility (SSRF, BL16B1). In SAXS sample preparation, a series of SPIO loaded micelles were lyophilized after separately centrifuged (10000 rpm for 2 h) in 1.5 mL micro centrifugal tube.

For the SAXS experiment, monochromatic x-rays (1.24 Å) with an energy of 10 keV were collected using a Rayonix MX225-HE detector (pixel size: 73.2 μm) and diffraction data was recorded using a MAR Research CCD area detector (pixel size: 80 μm). Two-dimensional SAXS images were reduced to the one-dimension form using angular integration and shown after background subtraction and normalization using the FIT2D. Scattering vectors (q) were calculated from the scattering angles (2θ) using $q = 4\pi/\lambda \sin(2\theta/2)$, where 2θ is the scattering angle and λ is the x-ray wavelength. The interparticle spacing (d) was calculated from the principal scattering maxima (q^*) using $d = 2\pi/q^*$.

2.4. Magnetization and T_2 relaxivity studies of polymer/SPIO nanocomposites

The lyophilized samples used for SAXS were carefully transferred to the appropriate holder for analysis of their magnetization using a physical property measurement system vibrating sample magnetometer (PPMS-VSM, Quantum Design, San Diego, U.S.). Hysteresis loops (−30 kOe–30 kOe) were collected at 300 K and normalized to the saturation magnetization.

T_2 relaxivities of SPIO loaded nanocomposites were measured at 1.5 T on a clinical MR scanner (Siemens Sonata) at room temperature. The T_2-weighted images were acquired with a conventional spin echo acquisition (TR = 5000 ms) with TE values ranging from 6 to 500 ms. Relaxivity values of r_2 were calculated through the curve fitting of $1/T_2$ relaxation time (s^{-1}) versus the iron concentration (mM).

3. Results and discussion

3.1. Synthesis and characterization of versatile anchors and the ligand exchange of SPIO nanocrystals

The gel permeation chromatography (GPC) (HLC-8320GPC, Japan) analyses revealed that the number-average molecular weight (Mn) of all polyesters (Bn_2-DA-PCL1k, Bn_2-DA-PCL2k, and Bn_2-DA-PLA1k) agrees well with their calculated values from ^{1}H NMR spectrum ($CDCl_3$), and typical results are summarized in Table 1. Subsequently, we

Table 1. Characteristics of the prepared DA-capping polymers with various molecular weight.

Samples	Mn[a] (Da)	Mw[a] (Da)	PDI	Mn[b] (Da)
Bn_2-DA-PCL1k	1273	1806	1.419	1130
Bn_2-DA-PCL2k	2160	3201	1.482	2145
Bn_2-DA-PLA1k	1091	1697	1.547	1065

[a]Measured by GPC; [b]calculated based on 1H NMR spectrum.

obtained the resulting product DA capping polymers after hydrogenation which function as a robust anchor for the replacement of the original SPIO ligands, because enediol ligands can bind strongly to iron atoms forming an octahedral geometry of oxygen-coordinated iron, which may result in a stable coating.[22]

As synthesized, these monodisperse SPIO (OA-SPIO) nanocrystals are coated with oleate/oleylamine, making them stable in hexane and some other nonpolar or weakly polar organic solvents. Comparison of the status before and after ligand exchange with DA-polyester, one can see that surface modified SPIO nanocrystals (collectively called DA-SPIO) were transferred to dimethylformamide (DMF) solution (at the bottom) from hexane solution (at the top) (see Fig. 3(a)), which suggested that DA-polyesters were introduced on the surface of SPIO nanocrystals and made them stably dispersed in polar solvent.

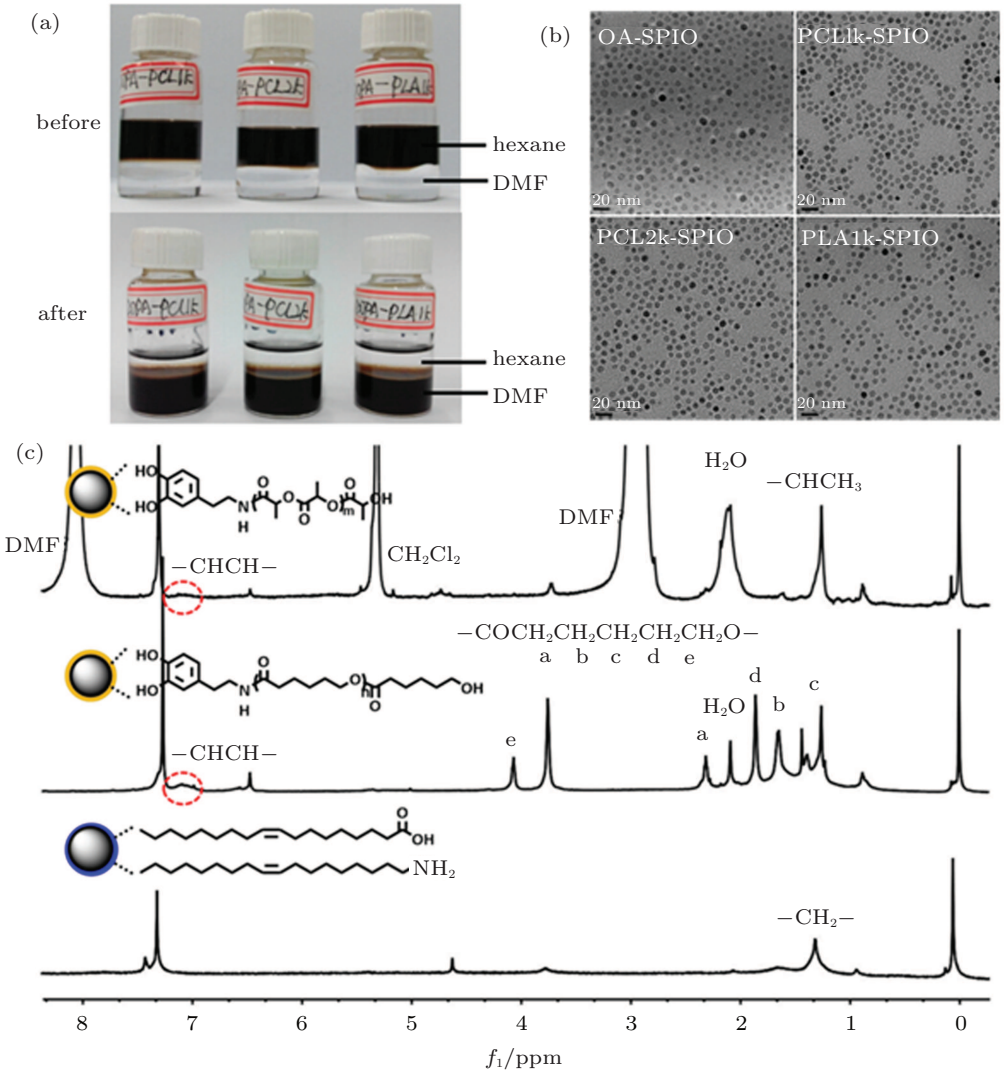


Fig. 3. (color online) (a) OA-SPIO nanocrystals were transferred to DMF solution (lower) from hexane (upper) after ligand exchange; (b) TEM images of SPIO nanocrystals before and after ligand exchange; (c) comparison of the ^{1}H HRMAS NMR spectra of surfactant-coated SPIO nanocrystals dispersed in $CDCl_3$ at a 5 kHz MAS rate.

In this context, we directly studied the chemical structure of organic molecules anchored onto the surface of SPIO nanocrystals via high-resolution magic-angle spinning (HRMAS) ^{1}H NMR spectroscopy. The HRMAS ^{1}H NMR spectra of SPIO nanocrystals dispersed in $CDCl_3$ were obtained with quite narrow and split signals corresponding to the characteristic protons of the covalently bound ligands at 5 kHz MAS rates (see Fig. 3(c)). These emphasize the fact that ligand exchange occurred upon exposure to the DA polyesters. DLS measurements (see Fig. 4) showed that before surface

modification, OA-SPIO nanocrystals in THF solution have an average hydrodynamic diameter of 7.8 ± 1.2 nm. After ligand exchange, the average hydrodynamic diameter of particles in THF solution equal to $\sim$ 12.4, 16.8, and 12.7 nm for PCL1k-SPIO, PCL2k-SPIO, and PLA1k-SPIO, respectively. The increase in the size of the DA-SPIO nanoparticles is ascribed to the increase in the coating thickness of highermolecular weights of polyesters than oleic acid and oleylamine. TEM images demonstrated that the nanoparticles are well dispersed both before or after ligand exchange (see Fig. 3(b)).

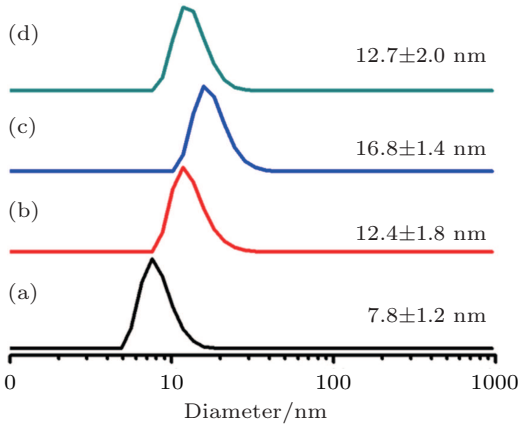


Fig. 4. (color online) DLS evaluation of (a) OA-SPIO; (b) PCL1k-SPIO; (c) PCL2k-SPIO; (d) PLA1k-SPIO in THF.

3.2. Self-assembly and characterization of nanocomposites

One viable method to control SPIO nanocrystals aggragation is self-assembly. The assembly process of copolymer/SPIO micelles was achieved through the slow addition of the THF mixture solution of SPIO nanocrystals and copolymers to water under sonication. The aggregate size control was achieved by adjusting the copolymer/SPIO naocrystal mass ratio. DLS measurement showed narrow distribution of hydrodynamic size of these composite micelles, and all micelles are in the range of around 60 nm for mPEG5k-PCL5k/SPIO micelles and 50 nm for mPEG5k-PLA5k/SPIO micelles (see Fig. 5). TEM images (see Fig. 6) exhibited morphology of dried micelles and provide direct aggregation state of SPIO nanoparticles. However, it is impractical to measure the interparticle spacing of neighbored SPIO nanocrystal through TEM.

3.3. Measurement of SPIO nanocrystal interparticle spacing

SAXS technique is an efficient analytical method which determines the structure of particle systems in terms of aggregate ordering, separation, and nanoparticle spacing within the aggregate. In this work, SAXS was applied to quantify SPIO nanocrystals interparticle spacing of the nanocomposites (Shanghai Synchrotron Radiation Facility, BL16B1). As shown in Fig. 7, the SAXS curves exhibited a well-defined structure peak which indicated the presence of a high degree of order in the electron density associated with the neighbouring SPIO nanocrystals. The length of the scattering vector q values, representing average interparticle spacing, shifted steadily downward with increased coating thickness, confirming the expected increase in spacing distance. According to the scattering peak for calculation (see Fig. 7(a)), the averaged center-to-center particle spacing (d (nm) = $2\pi/q*$) of the SPIO nanocrystals dried from organic phase was determined to be 6.04, 6.41, 8.05, and 6.10 nm for OA-SPIO, PCL1k-SPIO, PCL2k-SPIO, and PLA1k-SPIO samples, respectively.

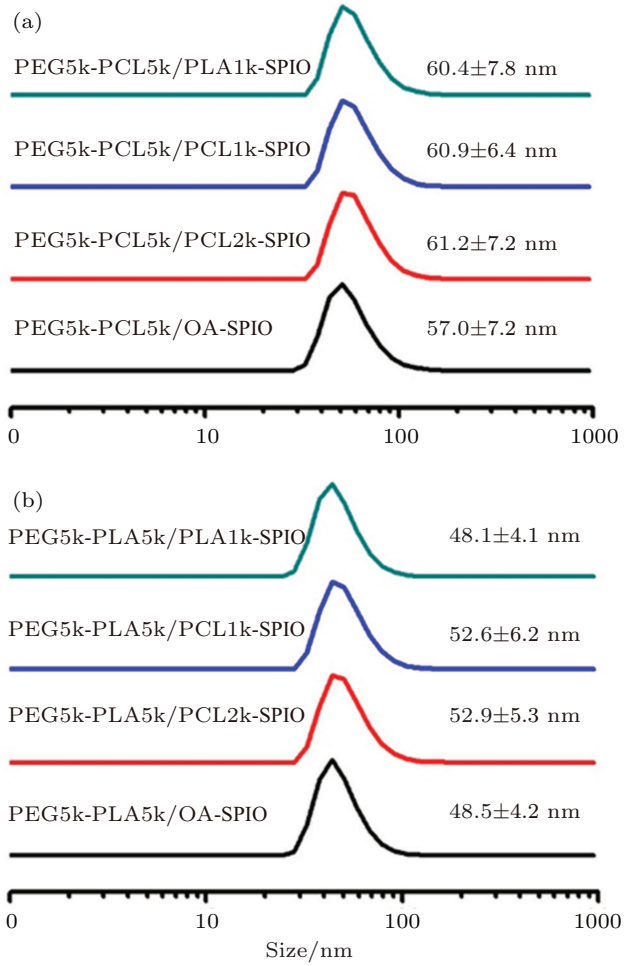


Fig. 5. (color online) DLS data of micelles in water loaded with SPIO nanocrystals which are coated with different polyesters.

As expected, the spacing values of the assembled samples (see Figs. 7(b) and 7(c)) separately showed a regular increase trend of interparticle spacing with the increasing shell thickness of SPIO nanocrystals. Comparison between SPIO loaded polymeric micelles based on PEG5k-PCL5k copolymers revealed that the interparticle spacing of SPIO nanocrystals increased from 6.28 nm for PEG5k-PCL5k/OA-SPIO micelles to 10.30 nm for PEG5k-PCL5k/PCL2k-SPIO micelles. Simultaneously, an overall increase of 1.71 nm was calculated between densely packed SPIO nanocrystals in the core

of PEG5k-PLA5k/PCL2k-SPIO micelles in comparison to that of PEG5k-PLA5k/OA-SPIO micelles, and the changing trend is slightly smaller than that of PEG5k-PCL5k/SPIO micelles. The exact reason is unknown, and the interaction between magnetic nanoparticles and PCL chains impedes the crystallization behavior of PCL in some degree.[14] Additionally, figure 7(d) illustrates the length of copolymer segments is a reason for considerable factor to affect the interparticle spacing of SPIO clusters.

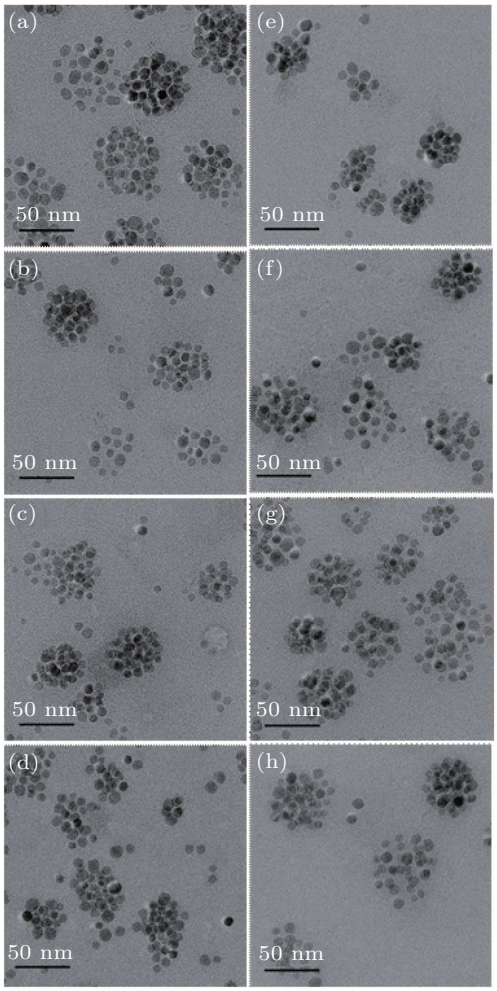


Fig. 6. TEM images of SPIO loaded micelles. (a) mPEG5k-PCL5k/OA-SPIO; (b) mPEG5k-PCL5k/PCL1k-SPIO; (c) mPEG5k-PCL5k/PCL2k-SPIO; (d) mPEG5k-PCL5k/PLA1k-SPIO; (e) mPEG5k-PLA5k/OA-SPIO; (f) mPEG5k-PLA5k/PCL1k-SPIO; (g) mPEG5k-PLA5k/PCL2k-SPIO; (h) mPEG5k-PLA5k/PLA1k-SPIO.

3.4. Magnetization and T_2 relaxivity of copolymer/SPIO nanocomposite

The intrinsic magnetization is an important parameter for SPIO nanoparticles' biomedical applications, because it has direct correlations with contrast efficacy of SPIO contrast agents. Figures 8(a) and 8(c) show magnetization curves of as-synthesized SPIO magnetic nanocomposites at 300 K. The insert in Fig. 8(a) is a magnification of the low field region of the magnetization curves. As shown in this figure,

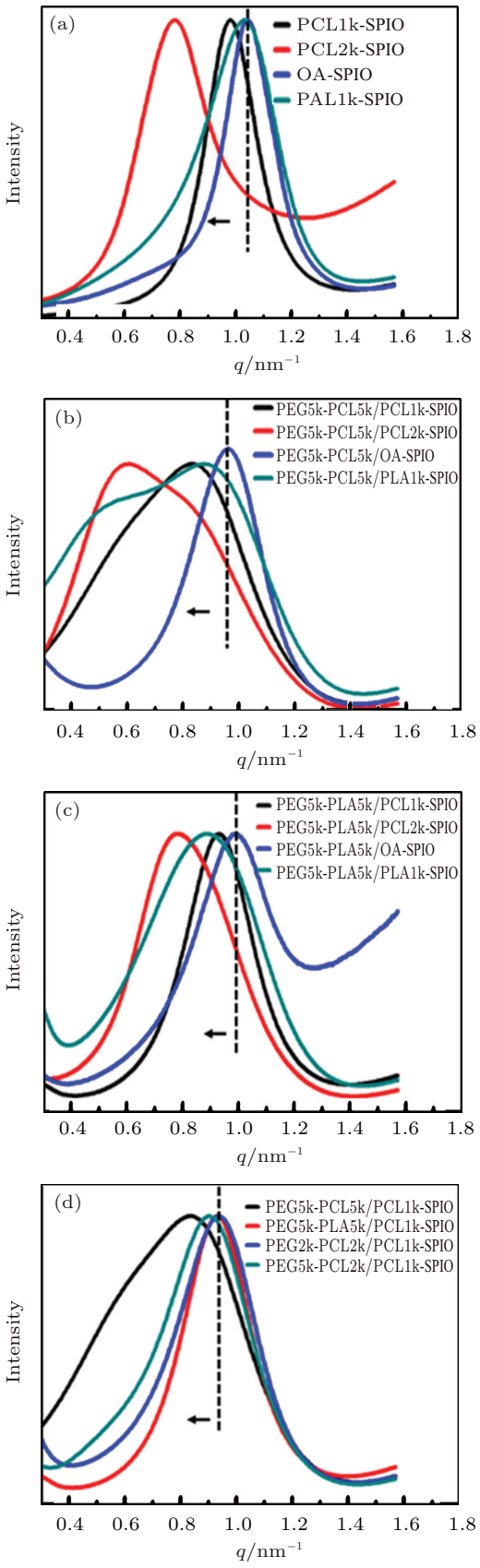


Fig. 7. (color online) SAXS plots shown after background subtraction and normalization. Scattering vector q values, representative of average interparticle spacing, shifted steadily downward representing the increase in spacing distance. Scattering vector q was calculated from the scattering angles (2θ) using $q = 4\pi/\lambda \sin(2\theta/2)$, where 2θ is the scattering angle and λ is the x-ray wavelength. SPIO interparticle spacing were calculated from the principal scattering maxima (q^*) using $d = 2\pi/q^*$.

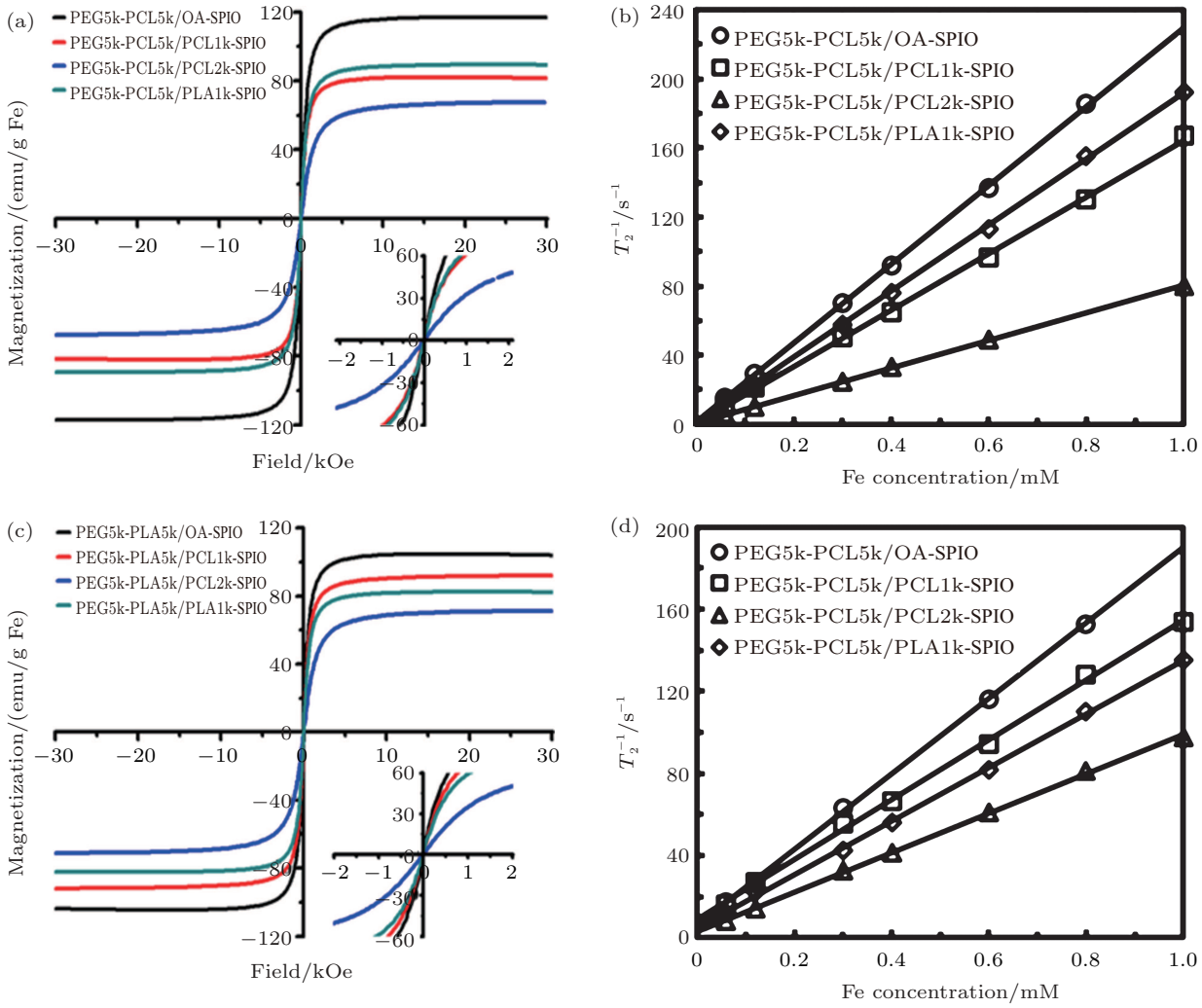


Fig. 8. (color online) The magnetic properties of SPIO clusters. (a), (c) Hysteresis loops of the SPIO nanoparticle containing micelles measured at 300 K (inset shows a zoomed-in plot between −2 kOe and 2 kOe magnetic field). (b), (d) T_2 relaxation rate ($1/T_2$, s^{-1}) as a function of iron concentration (mM) for SPIO micelles at 1.5 T. The M_s and T_2 relaxivities of SPIO clusters followed an descending trend with the increase of SPIO interparticle spacing.

there is no sign of magnetic remanence or coercivity which indicated the superparamagnetic nature of these SPIO clusters. However, magnetization curves showed different magnetic performances of the powders as a function of SPIO interparticle spacing in the core of micelles. The saturation magnetization value (M_s) of SPIO-loaded mPEG5k-PCL5k micelles changes from 116 to 89, 81, and 68 emu/g Fe with increasing SPIO interparticle spacing, respectively, due to the decrease of the magnetite fraction in each nanocluster, and such a trend was clearly observed from the magnetization curves of SPIO-loaded mPEG5k-PLA5k micelles (Table 2). These experimental results are in good agreement with the theoretical finding that M_s is roughly proportional to the density of magnetic nanocrystals within each nanocluster.[23] Furthermore, it is particularly noteworthy that the particle size is another important factor contributing to the magnetization property. The maximum value of M_s was 116 emu/g Fe for sample mPEG5k-PCL5k/SPIO micelles with a relatively large particle size.

The correlation analysis of SPIO interparticle spacing and T_2 relaxivities of these SPIO clusters were also observed from Figs. 8(b) and 8(d). Overall, T_2 relaxivities of both types of micelles (mPEG5k-PCL5k and mPEG5k-PLA5k) decreased dramatically with the increase in SPIO interpartice spacing, respectively. For instance, r_2 value of mPEG5k-PCL5k/OA-SPIO micelles was 227 Fe $mM^{-1}\cdot s^{-1}$, while that of mPEG5k-PCL5k/PCL2k-SPIO micelles reduced to 80 Fe $mM^{-1}\cdot s^{-1}$, due to the increase in SPIO interparticle spacing. T_2 relaxivities of SPIO-loaded mPEG5k-PLA5k micelles changed from 103 to 91, 85, and 71 Fe $mM^{-1}\cdot s^{-1}$ with increasing SPIO interparticle spacing, respectively (Table 2). It is reported that different coating ligands and coating layer thickness can affect magnetic spin anisotropy and ultimately r_2 relaxivity of magnetic nanoparticles.[24] Among these micelles, mPEG5k-PCL5k/OA-SPIO micelles with a mean size of 57 nm exhibited the highest relaxivity. In addition, with the increase of SPIO interparticle spacing, their relaxivity and saturation magnetization both revealed a descending trend. This result suggests that M_s of magnetic nanoclusters affect MRI signal intensity enhencement capabilities, and higher M_s resulted in much higher T_2 relaxivity.

Table 2. Summaries of magnetic property data of all resultant nanocomposites.

Samples	d /nm	M_s /(emu/g Fe)	r_2 /(Fe mM^{-1}·s^{-1})
PEG5k-PCL5k/OA-SPIO	6.54	116	227
PEG5k-PCL5k/PCL1k-SPIO	7.48	81	163
PEG5k-PCL5k/PCL2k-SPIO	10.30	68	80
PEG5k-PCL5k/PLA1k-SPIO	7.14	89	191
PEG5k-PLA5k/OA-SPIO	6.34	103	184
PEG5k-PLA5k/PCL1k-SPIO	6.75	92	145
PEG5k-PLA5k/PCL2k-SPIO	8.05	71	96
PEG5k-PLA5k/PLA1k-SPIO	7.14	84	131

4. Conclusions

In this study, monodisperse SPIO nanocrystals with different surface coating materials were prepared via ligand exchange reaction, and encapsulation of these nanocrystals inside polymer micelles could modulate SPIO nanocrystal interparticle spacing and the magnetic behaviors of their clusters. The current work demonstrated that the hydrodynamic size of SPIO nanocrystals increased with their surface coating thickness. Moreover, the assembly of these SPIO nanocrystals directly modulated the magnetic relaxation behaviors of their clusters. The M_s and T_2 relaxivities of SPIO clusters followed an increasing trend with the reduction of SPIO interparticle spacing.

Acknowledgment

The authors acknowledge Shanghai Synchrotron Radiation Facility (SSRF) for providing great support for SAXS measurements.

References

[1] Iliff J J, Lee H, Yu M, Feng T, Logan J, Nedergaard M and Benveniste H 2013 *J. Clin. Invest.* **123** 1299
[2] Jin R, Lin B, Li D and Ai H 2014 *Curr. Opin. Pharmacol.* **18** 18
[3] Nathan P, Zweifel M, Padhani A R, Koh D M, Ng M, Collins D J, Harris A, Carden C, Smythe J, Fisher N, Taylor N J, Stirling J J, Lu S P, Leach M O, Rustin G J S and Judson I 2012 *Clin. Cancer Res.* **18** 3428
[4] Sourbron S, Sommer W H, Reiser M F and Zech C J 2012 *Radiology* **263** 874
[5] Wang D, Su H, Liu Y, Wu C, Xia C, Sun J, Gao F, Gong Q, Song B and Ai H 2012 *Chin. Sci. Bullet* **57** 4012
[6] Wang D, Lin B B and Ai H 2014 *Pharm. Res.-Dordr* **31** 1390
[7] Shokrollahi H 2013 *Mat. Sci. Eng. C-Mater.* **33** 4485
[8] Lin B, Su H, Jin R, Li D, Wu C, Jiang X, Xia C, Gong Q, Song B and Ai H 2015 *Sci. Bullet* **60** 1272
[9] Su H Y, Wu C Q, Li D Y and Ai H 2015 *Chin. Phys. B* **24** 127506
[10] Jasanoff A 2007 *Curr. Opin Neurobiol.* **17** 593
[11] Xie J, Liu G, Eden H S, Ai H and Chen X Y 2011 *Accounts Chem. Res.* **44** 883
[12] Lee N and Hyeon T 2012 *Chem. Soc. Rev.* **41** 2575
[13] Jun Y W, Lee J H and Cheon J 2008 *Angew. Chem. Int. Ed.* **47** 5122
[14] Lu J, Ma S L, Sun J Y, Xia C C, Liu C, Wang Z Y, Zhao X N, Gao F B, Gong Q Y, Song B, Shuai X T, Ai H and Gu Z W 2009 *Biomaterials* **30** 2919
[15] Paquet C, de Haan H W, Leek D M, Lin H Y, Xiang B, Tian G H, Kell A and Simard B 2011 *Acs Nano* **5** 3104
[16] Su H Y, Liu Y H, Wang D, Wu C Q, Xia C C, Gong Q Y, Song B and Ai H 2013 *Biomaterials* **34** 1193
[17] Poselt E, Kloust H, Tromsdorf U, Janschel M, Hahn C, Masslo C and Weller H 2012 *Acs Nano* **6** 1619
[18] Tromsdorf U I, Bigall N C, Kaul M G, Bruns O T, Nikolic M S, Mollwitz B, Sperling R A, Reimer R, Hohenberg H, Parak W J, Forster S, Beisiegel U, Adam G and Weller H 2007 *Nano Lett.* **7** 2422
[19] Taktak S, Sosnovik D, Cima MJ, Weissfeder R and Josephson L 2007 *Anal. Chem.* **79** 8863
[20] Frankamp BL, Boal AK, Tuominen M T and Rotello V M 2005 *J. Am. Chem. Soc.* **127** 9731
[21] Sun S H, Zeng H, Robinson D B, Raoux S, Rice P M, Wang S X and Li G X 2004 *J. Am. Chem. Soc.* **126** 273
[22] Xu C J, Xu K M, Gu H W, Zheng R K, Liu H, Zhang X X, Guo Z H and Xu B 2004 *J. Am. Chem. Soc.* **126** 9938
[23] Matsumoto Y and Jasanoff A 2008 *Magn. Reson. Imaging* **26** 994
[24] Tong S, Hou S J, Zheng Z L, Zhou J and Bao G 2010 *Nano Lett.* **10** 4607